

A total strain-based hysteretic material model for reinforced concrete structures: theory and verifications

Gun Jin Yun*

Department of Civil Engineering, The University of Akron, Akron, OH, 44325-3905, USA

Thomas G. Harmon[‡], Shirley J. Dyke^{††} and Migeum So^{‡‡}

Department of Mechanical, Aerospace and Structural Engineering, Washington University in St. Louis, St. Louis, MO, 64130, USA

(Received September 21, 2007, Accepted June 23, 2008)

Abstract In this paper, a total strain-based hysteretic material model based on MCFT is proposed for non-linear finite element analysis of reinforced concrete structures. Although many concrete models have been proposed for simulating behavior of structures under cyclic loading conditions, accurate simulations remain challenging due to uncertainties in materials, pitfalls of crude assumptions of existing models, and limited understanding of failure mechanisms. The proposed model is equipped with a fully generalized hysteresis rule and is formulated for 2D plane stress non-linear finite element analysis. The proposed model has been formulated in a tangent stiffness-based finite element scheme so that it can be used for most general finite element analysis packages. Moreover, it eliminates the need to check that tensile stresses can be transmitted across a crack. The tension stiffening model is a function of the bar orientation and any orientation can be accommodated. The proposed model has been verified with a series of experimental results of 2D RC planar panels. This study also demonstrates how parameters of the proposed model associated with cyclic damage modeling influences the pinched cyclic shear behavior.

Keywords: hysteretic material constitutive model; reinforced concrete; non-linear finite element analysis; tangent stiffness-based formulation; hysteretic behavior; cyclic loading.

1. Introduction

Predictions of ultimate strength and ductility under general loading conditions are very important for seismically resistant design of reinforced concrete structures. For sufficiently accurate simulations, realistic material constitutive models are required with reliable numerical procedures. Although many concrete models have been proposed for simulating behavior of structures (Cotsovos and Pavlovic 2005, He, *et al.* 2006, Kim, *et al.* 2002, Kwak and Kim 2004, Noh and Choi 2006), accurate simulations under cyclic loading conditions remain challenging due to uncertainties in

* Assistant Professor, Corresponding Author, Email: gy3@uakron.edu

‡ Professor, E-mail: tharm@seas.wustl.edu

†† Professor, E-mail: gdyke@wustl.edu

‡‡ Graduate Research Assistant, E-mail: salt-lighter@yahoo.com

materials, simplifying assumptions of existing models, limited understanding of failure mechanisms pertaining to pinched behavior, difficulty in modeling accumulated damage through unloading and reloading excursions, and crack-closing and reopening mechanisms. In particular, the ambiguity on transitions between different stress states stems from lack of sufficient experimental data.

Over the last two decades, several cyclic concrete models have been proposed for non-linear finite element analysis of reinforced concrete structures. Early on, plasticity-based models were investigated because of their rigorous mathematical theory (Chen 1988, De Borst and Feenstra 1995). Although plasticity models can provide well-defined loading and unloading criteria (Kratzig and Polling 2004, Park and Kim 2005), degradation of stiffness and strength during reloading phase can not be described due to the fundamental assumption of a continuum. In 1986, Vecchio and Collins proposed a modified compression field theory (MCFT) focusing on shear-dominant behavior of a 2D planar panel element as a non-linear elasticity model. Following MCFT, in 1999, Vecchio proposed a cyclic model of reinforced concrete structures based on a smeared rotating crack concept. Although this is a significant step forward, comparisons with an experimental panel test result showed a large discrepancy in terms of shear stress-strain hysteric behavior partially because of crude damage modeling in principal stress-strain behavior. Recently, Palermo and Vecchio (2003, 2004) proposed an improved cyclic model including non-linear unloading, damage modeling in reloading branches, and rationally determined residual strains both in compression and tension. The model has been verified in terms of macroscopic behavior of shear wall structures where the behavior is largely affected by yielding of reinforcement (Palermo and Vecchio 2007). Although Palermo's model provides rational empirical equations based on experimental observations, it has been observed that the empirical equations for non-linear unloading states cause numerical instabilities in some strain ranges. The model is implemented into a secant stiffness-based finite element algorithm. Based on Modified Compression Field Theory, Stevens, *et al.* (1991a, 1991b) proposed a rational cyclic material model which is suitable for finite element implementation. Particularly, the modified average tensile response eliminates the need to check that tensile stresses can be transmitted across a crack and allows for arbitrary orientation of reinforcement. However, the Stevens' model has not been empirically verified beyond the yielding of the steel reinforcements.

The University of Houston research group headed by Hsu also developed a series of rational concrete models using extensive experimental programs. These include the Rotating Angle Softened Truss Model (RA-STM) (Belarbi and Hsu 1994, 1995), the Fixed Angle Softened Truss Model (FA-STM) (Hsu and Zhang 1997, Pang and Hsu 1996, Zhang and Hsu 1998, Zhu and Hsu, *et al.* 2001) and the Softened Membrane Model (SMM) (Hsu and Zhu 2002). Although FA-STM was implemented in a non-linear finite element program, it was only tested under monotonic loading conditions (Wang and Hsu 2001). As an extension of SMM, the Cyclic Softened Membrane Model (CSMM) for reinforced concrete has recently been proposed and experimentally verified (Mansour and Hsu 2005a, Mansour and Hsu, 2005b, Mansour and Lee, *et al.* 2001). These models have been implemented in a general non-linear finite element program (Zhong 2005) and tested with 1-D element under cyclic loading conditions and 2-D element under monotonically increasing shear loading (Hsu and Mansour, *et al.* 2006).

In this paper, a total strain-based hysteretic material constitutive model for reinforced concrete based on MCFT is proposed to complement the current gaps in available modeling techniques. The proposed model is equipped with a fully generalized hysteresis rule and formulated for 2D plane stress non-linear finite element analysis. It is an extension of Palermo's model combined with Stevens' approach for average tensile responses. Therefore, the smeared rotating crack assumption

has been made for the proposed model. Although secant stiffness-based FE formulation has been successfully used for the MCFT implementation (Vecchio 1999), the tangent stiffness based formulation has been adopted in this paper because it is more common in commercial programs. Therefore, the proposed model has been formulated using tangent stiffness and thus is easily adopted in most general finite element packages. This study also presents important generalizations on how different cyclic damage model parameters influence pinched cyclic shear behavior.

2. Research significance

Further development to improve hysteretic material constitutive models is essential to more accurately predict the capacity of reinforced concrete structures under general loading conditions. Although there are several cyclic material constitutive models, the experimental conditions used to develop these are different and thus generalization of these models is limited. Furthermore, none of them have been verified at both the element level and the structural level.

This paper presents a new total strain-based hysteretic material model which can easily be implemented into non-linear finite element codes to provide more accurate simulations of reinforced concrete structures (or walls) under cyclic loading conditions. In addition to its verification using experimental data, this paper presents the characterizations of damage, including unloading-reloading models and crack-closing/reopening models, and their effects on pinched shear behavior.

3. Material constitutive model for concrete

The proposed total strain-based material model is based on MCFT and suitable for reinforced concrete panels under in-plane shear and normal stress states. It quantifies compression softening of the cracked concrete under coexisting transverse tensile strain. The proposed model assumes coincidence of the principal strain direction with the principal stress direction. Accordingly, it adopts a smeared rotating crack approach with refined hysteretic rules defining stress-strain relationship for crack-closing and reopening. Because a tensile backbone curve can be shifted into a compressive strain region due to compressive residual strain under general loading conditions, stress states are determined by current principal stresses instead of strains. The following describes tensile and compressive responses of the proposed model in terms of principal stresses and strains.

3.1. Tension model under monotonic loading

The proposed model for tensile behavior of the concrete is described in terms of average stresses and strains. While the stresses in plain concrete drop to zero after cracking, the reinforced concrete can carry tensile stresses even after cracking due to bond transfer between reinforcements and surrounding concrete. This effect is referred to as tension stiffening. Tension stiffening is known to be influenced by many factors such as reinforcement ratio, reinforcement orientation, distribution and spacing of cracks, and interface bond transfer. Additionally, the tension stiffening can be affected by local mechanisms such as the breakdown of aggregate interlock along the crack surface, fractures of the reinforcement across the crack, and residual straining due to concentrated yielding at the crack, etc. The proposed model adopts a tension stiffening model developed by Stevensk, *et al.*

(1991b). One advantage of the tension stiffening model is that it eliminates the need for stress check presented in the original MCFT implementation; that is, the finite element program does not have to check if the reinforcement stress at the cracks exceeds the yield stress (Stevens, *et al.* 1991b).

Before cracking, the concrete is assumed to show a linearly elastic behavior as follows

$$\sigma_c = E_1 \varepsilon_c \quad (1)$$

where E_1 is the linear elastic tangent stiffness and σ_c and ε_c indicate the concrete stress and strain, respectively. The uni-axial tensile response of concrete after cracking can be described by

$$\sigma_c = \sigma_{cr} [(1 - \eta) e^{-\lambda_1 (\varepsilon_c - \varepsilon_{cr})} + \eta] \quad (2)$$

where σ_{cr} and ε_{cr} are the concrete stress and strain at cracking, respectively, and η is the coefficient for the total force transferred to concrete. The value of η is related to the bond characteristics of the reinforcement being used and is expressed as follows.

$$\eta = 75 \cdot \frac{\rho_s}{d_b} \quad (3)$$

where ρ_s is the steel reinforcement ratio and d_b is the diameter of the reinforcement. The parameter λ_1 controls the rate of decay of the response after cracking. As shown in Fig. 1, a larger amount of well-distributed reinforcement causes lower rate of tensile stress decay after cracking. The parameter λ_1 is given as

$$\lambda_1 = \frac{270}{\sqrt{\eta}}; \quad \lambda_1 \leq 1000 \quad (4)$$

For the case of biaxial behavior, the parameter η is modified to account for the orientation of the principal tensile strain relative to various reinforcement groups. The modified parameter is expressed as

$$\eta = \sum_{i=1}^n \left[\cos^2 \Delta\theta_i + \sin^2 \left(\frac{4\Delta\theta_i^2}{\pi} \right) \right] \eta_i \quad (5)$$

where $\Delta\theta_i = \theta - \theta_i$; θ indicates the principal tensile strain direction; n is the total number of reinforcement groups and θ_i the orientation of the i th reinforcement group, and η_i is calculated for the i th group by Eq. (3). The second term in Eq. (5) accounts for an increase in average concrete tensile stress due to the complex interactions between reinforcement and concrete at the cracks such

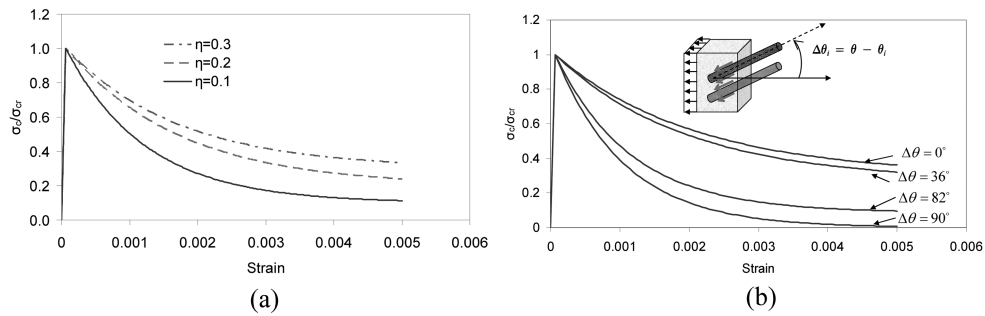


Fig. 1 Stress-strain envelop for concrete in tension after cracking

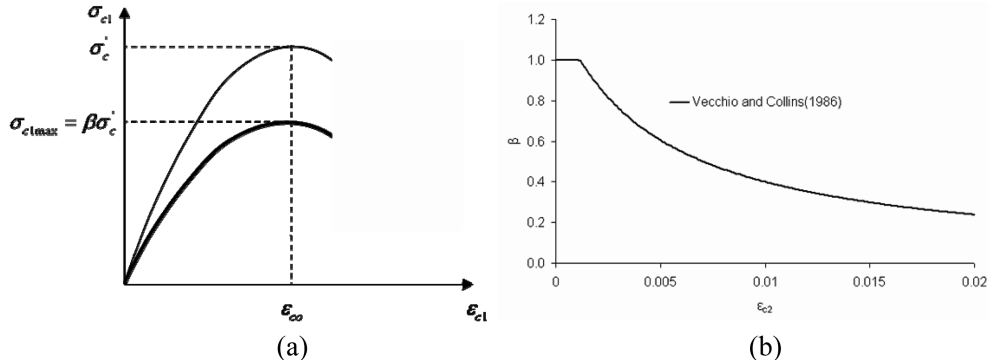


Fig. 2 (a): Degradation of compressive strength of cracked concrete (b): Softening Coefficient for Cracked Concrete

as dowel action and aggregate interlock. Fig. 1(b) shows comparisons of the post-cracking tensile behavior with different orientations. As observed by Fig. 1(b), as the angle of the rebar is closer to 90 degrees, the average tensile stress drastically drops.

3.2. Compression model under monotonic loading

Concrete exhibits a significantly different strength envelope depending on the biaxial state of stress. As discussed previously, stress states are determined by current principal stress states due to a potential shift of the tensile backbone curve under general loading conditions.

3.2.1. Tension-compression stress state

In the original MCFT model, a softening coefficient which is a function of the transverse tensile strain is applied to peak compressive stress alone. However, a wide spectrum of the softening coefficients has been suggested by various researchers (Belarbi and Hsu 1991, Mikame, *et al.* 1991), showing good correlation with experimental data. In this study, a parabolic compressive stress envelop from the original MCFT model suggested by Vecchio and Collins (1986) is adopted as shown in Fig. 2. The parabolic relationship is given by

$$\sigma_{c1} = \sigma'_{c1max} \left[2 \frac{\epsilon_{c1}}{\epsilon_{co}} - \left(\frac{\epsilon_{c1}}{\epsilon_{co}} \right)^2 \right] \quad (6)$$

where σ_{c1} is the compressive principal stress; ϵ_{c1} is the compressive principal strain; ϵ_{co} is the strain at the peak compressive stress. The coefficient σ'_{c1max} is expressed as

$$\sigma'_{c1max} = \beta \sigma'_c = \frac{\sigma'_c}{0.84 - 0.34 \frac{\epsilon_{c2}}{\epsilon_{co}}} \quad (7)$$

where ϵ_{c2} indicates the tensile principal strain in normal direction to compressive principal strain direction and σ'_c is the compressive strength of the concrete.

3.2.2. Compression-compression stress state

For concrete under biaxial compressive stress states, the compressive strength is enhanced by the confining effect. The strength surface suggested by Vecchio (1992) was obtained by approximating the results from a comprehensive experimental study carried out by Kupfer *et al.* (1969). Although other accurate models for confined concrete are available (Kent and Park 1971, Scott, *et al.* 1982), they are more complicated. Therefore, their parabolic compressive envelop is adopted with following strength enhancement factors

$$K_{c1} = 1.0 + 0.92 \left(\frac{\sigma_{c2}}{\sigma_c'} \right) - 0.76 \left(\frac{\sigma_{c2}}{\sigma_c'} \right)^2$$

$$K_{c2} = 1.0 + 0.92 \left(\frac{\sigma_{c1}}{\sigma_c'} \right) - 0.76 \left(\frac{\sigma_{c1}}{\sigma_c'} \right)^2$$
(8)

where K_{c1} and K_{c2} are the strength enhancement factors for concrete in the 1 and 2-directions, respectively. Multiplying the strength and the strain at the peak stress by the factors yields

$$\sigma_{p1} = K_{c1} \sigma_c'; \quad \varepsilon_{p1} = K_{c1} \varepsilon_{co}$$
(9)

Then, the ascending and descending curve in the 1-direction can be obtained as

$$\sigma_{c1} = \sigma_{p1} \left[2 \left(\frac{\varepsilon_{c1}}{\varepsilon_{p1}} \right) - \left(\frac{\varepsilon_{c1}}{\varepsilon_{p1}} \right)^2 \right] \quad \text{for } \varepsilon_{p1} < \varepsilon_{c1} < 0.0$$

$$\sigma_{c1} = \sigma_{p1} \left[1 - \left(\frac{\varepsilon_{c1} - \varepsilon_{p1}}{2\varepsilon_{co} - \varepsilon_{p1}} \right)^2 \right] \quad \text{for } 2\varepsilon_{co} < \varepsilon_{c1} < \varepsilon_{p1}$$
(10)

Similarly, concrete stress in the 2-direction can be obtained by replacing ε_{c1} , ε_{p1} and σ_{p1} with corresponding values in the 2-direction. The compressive stress envelope and strength surface are shown in Fig. 3. This relationship is used for simplicity and underestimates the ductility of confined concrete.

3.3. Hysteretic stress-strain relationships under general loading

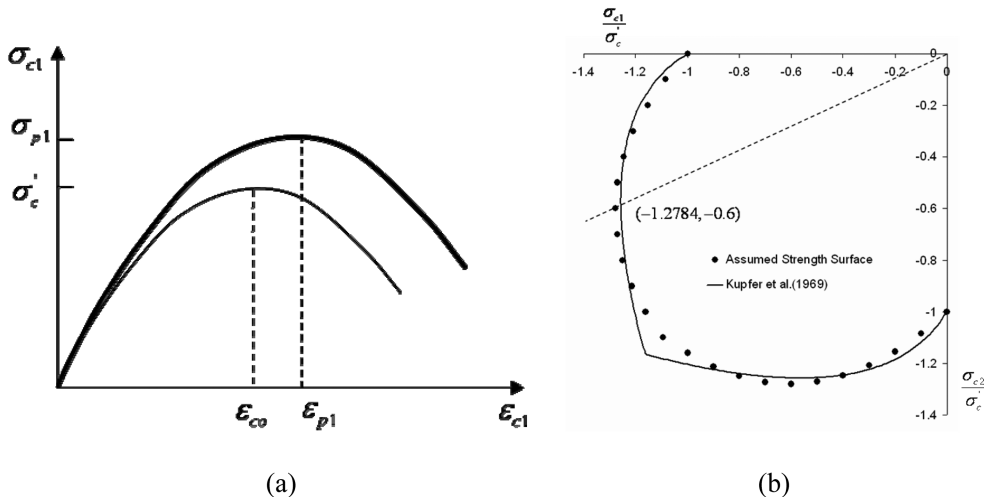


Fig. 3 Compression response under biaxial stress state: (a) Confining effect of concrete in 1-direction (b) Comparison between assumed strength surface under biaxial compressive loading and Kupfer's surface

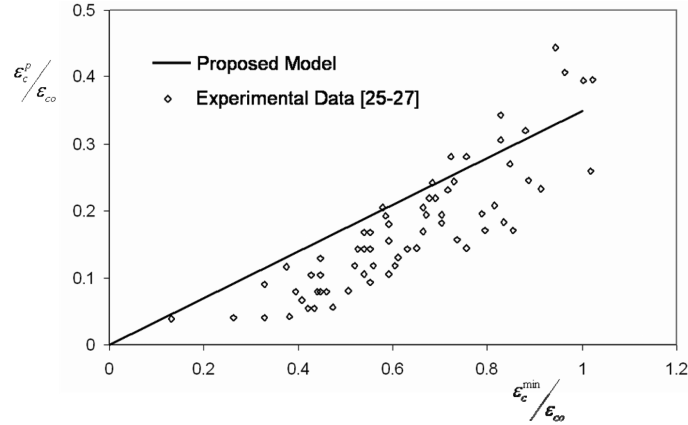


Fig. 5 Plastic offset model for concrete in compressive hardening region

$$\sigma_c = \sigma_c^{\min} + E_{c2}(\epsilon_c - \epsilon_c^{\min}) + \left[\frac{(E_{c3} - E_{c2})(\epsilon_c - \epsilon_c^{\min})}{N(\epsilon_c^p - \epsilon_c^{\min})} \right] \quad \text{for } \epsilon_c < \epsilon_{co} \quad (12)$$

where σ_c and ϵ_c are the instantaneous stress and strain in the concrete on the unloading curve. E_{c2} is a tangent stiffness value which is equal to the initial tangent stiffness E_c . E_{c3} is assumed to be $0.071E_c$. The value of N is defined as

$$N = \frac{(E_{c3} - E_{c2})(\epsilon_c^p - \epsilon_c^{\min})}{\sigma_c^{\min} + E_{c2}(\epsilon_c^p - \epsilon_c^{\min})} \quad (13)$$

where ϵ_c^p is the plastic offset strain as shown in Fig. 4. The plastic offset strain is described as

$$\epsilon_c^p = \epsilon_{co} \left[0.166 \left(\frac{\epsilon_c^{\min}}{\epsilon_{co}} \right) + 0.132 \left(\frac{\epsilon_c^{\min}}{\epsilon_{co}} \right)^2 \right] \quad \text{for } \epsilon_c < \epsilon_{co} \quad (14)$$

$$\epsilon_c^p = 0.35 \epsilon_c^{\min} \quad \text{for } \epsilon_{co} < \epsilon_c$$

The reloading stiffness in the softening region, the degradation of the reloading stiffness, and the partial unloading/reloading rule follow Palermo's model (2003). The unique advantage of the model is that it considers degradation of reloading stiffness as the minimum unloading strain is updated during the load cycling.

3.3.2. Tension model under general loading

In 1999, Vecchio used a tension model under cyclic loading which adopts linear unloading and reloading stiffness without plastic offset strain (Vecchio 1999). Other researchers proposed different hysteretic models for non-linear responses in the tension regime under cyclic loading (Stevens, *et al.* 1987). Palermo also proposed a tension stiffening model under cyclic loading, based on the compression model (Palermo and Vecchio 2003). Because hysteretic behavior in tension is influenced by many factors such as bond force transfer, orientation of reinforcement, steel ratio, and loading type, their mechanisms are very complex. Moreover, because each model has been developed based on different experimental results and assumptions, there is still a room for further improvement. In this study, Palermo's empirical equation for hysteretic response in tension has been

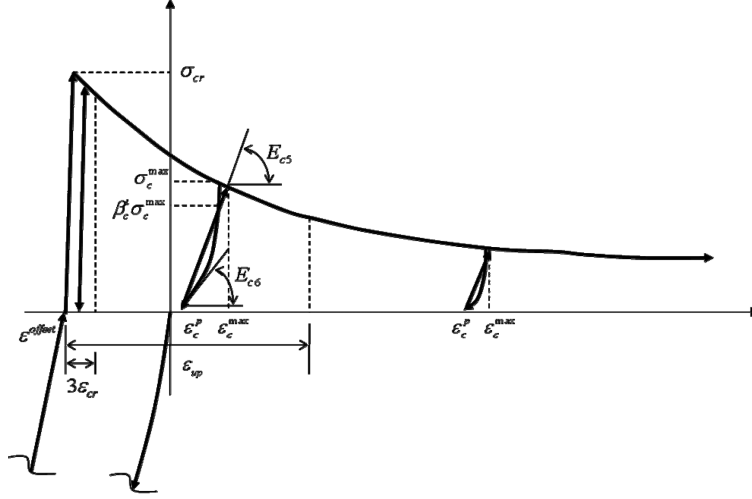


Fig. 6 Hysteretic stress-strain curves with offset strain in tension

modified to eliminate the numerical problems resulting in certain strain ranges.

The unloading stiffness of the proposed model takes an initial tangent stiffness (E_c) for the unloading and reloading stiffness as

$$\sigma_c = E_c(\varepsilon_c - \varepsilon_0) + \sigma_0 \quad \text{for } 0.0 < \varepsilon_c < 3\varepsilon_{cr} \quad (15)$$

where ε_{cr} indicates the crack strain ($= \sigma_{cr}/E_c$) of the concrete; σ_0 and ε_0 are the current stress and strain at the last converged point. Although data from several experiments (Yankelevsky and Reinhardt 1989) are available to formulate the plastic offset strain in tension regime, no test data is available in the large strain range (strains greater than 0.002). Therefore, the proposed model sets an upper bound ($\varepsilon_{up}=0.00275$) on tensile strain to determine plastic offset strain as in Eq. (18). The concrete stress is determined by the following equation

$$\sigma_c = \sigma_c^{\max} - E_{c5}(\varepsilon_c^{\max} - \varepsilon_c) + \left[\frac{(E_{c5} - E_{c6})(\varepsilon_c^{\max} - \varepsilon_c)^N}{N(\varepsilon_c^{\max} - \varepsilon_c)^{N-1}} \right] \quad (16)$$

where σ_c and ε_c are the instantaneous stress and strain in the concrete on the unloading curve. E_{c5} is a tangent stiffness value which is equal to the initial tangent stiffness E_c . E_{c6} is assumed to take the same form as Palermo's model. The value of N is defined as

$$N = \frac{(E_{c5} - E_{c6})(\varepsilon_c^{\max} - \varepsilon_c^p)}{E_{c5}(\varepsilon_c^{\max} - \varepsilon_c^p) - \sigma_c^{\max}} \quad (17)$$

where the plastic offset strain is suggested as

$$\begin{aligned} \varepsilon_c^p &= 146(\varepsilon_c^{\max} - \varepsilon^{\text{offset}})^2 + 0.523(\varepsilon_c^{\max} - \varepsilon^{\text{offset}}) \quad \text{for } 3\varepsilon_{cr} < \varepsilon_c < \varepsilon_{up} \\ \varepsilon_c^p &= 0.95(\varepsilon_c^{\max} - \varepsilon^{\text{offset}}) \quad \text{for } \varepsilon_{up} \leq \varepsilon_c \end{aligned} \quad (18)$$

and $\varepsilon^{\text{offset}}$ is the offset strain where the tension stress is first generated and ε_{up} is the upper bound of

tensile strain which is equal to 0.00275. The offset strain ($\varepsilon^{\text{offset}}$) is dependent on hysteretic loading conditions.

The proposed model is different from Palermo's model (Palermo and Vecchio 2003) in that it modifies the unloading and reloading stiffness and includes degradation of reloading stiffness and partial unloading/reloading rules. As presented in the compression model, a unique advantage of the model is that it can consider degradation of reloading stiffness as the minimum unloading strain is updated during load cycling.

3.3.3. Transition between tension and compression models

Under a general hysteretic loading condition, reinforced concrete is under a repeated crack-closing and reopening process throughout the loading history. When cracked concrete is under a crack-closing excursion, the cracks may not be completely closed for various reasons. Therefore, compressive stresses may develop even when cracks are not completely closed. A variation of the stiffness under crack closing can be caused by crushing of the crack surface roughness and by bond-slip between the reinforcement and the surrounding concrete, etc. However, for simplicity, the proposed model uses linear crack-closing stiffness as a function of the plastic offset strain and therefore does not include the energy dissipation effect. The model is described as

$$\begin{aligned}\sigma_{c\text{close}} &= E_c(\alpha\varepsilon_c^{\text{max}} + \gamma) \\ \sigma_c &= \frac{\sigma_{c\text{close}}}{\varepsilon_c^p}(\varepsilon_c - \varepsilon_0) + \sigma_0\end{aligned}\quad (19)$$

where α and γ are the steepness coefficients for the crack closing stiffness which are initially set to 0.0016 and 50.0×10^{-6} . However, the parameters can be calibrated to experimental data as will be shown and $\sigma_{c\text{close}}$ is the compressive stress when cracks are completely closed.

For the crack-reopening model, some of the existing models adopted zero-stiffness until re-entering the tensile regime (Elmorsi, *et al.* 1998, Vecchio 1999). However, a linear crack-reopening stiffness is assumed for the proposed model. Stresses along the cracking reopening curve can be obtained as

$$\sigma_c = \left(\frac{\beta_c^t \sigma_c^{\text{max}} - \sigma_{ro}^{\text{min}}}{\varepsilon_c^{\text{max}} - \varepsilon_{ro}^{\text{min}}} \right) (\varepsilon_c - \varepsilon_{ro}^{\text{min}}) + \sigma_0 \quad (20)$$

where σ_c^{max} and $\varepsilon_{ro}^{\text{min}}$ are the stress and strain at a reversed reloading point as shown in Fig. 7. σ_{ro}^{min} could be non-zero depending on the load step size. β_c^t indicates a damage parameter in the tensile regime, which is expressed as

$$\beta_c^t = \frac{1}{1 + 1.15(\varepsilon_c^{\text{max}} - \varepsilon_{ro}^{\text{min}})^{0.25}} \quad (21)$$

It is noteworthy that the crack closing and reopening mechanism has a significant effect on pinching behavior of shear stress-strain relationship in modeling shear failure-dominant structures.

Fig. 8 shows the schematic hysteresis rule adopted in the proposed model. Fig. 8(a) demonstrates a typical uni-axial hysteretic stress-strain relationship which starts with tensile loading and then moves to the compression regime. For the non-cracked region, from point *a* to *b*, the response follows the linear elastic behavior given by Eq. (15) until cracking occurs. After the cracking stress

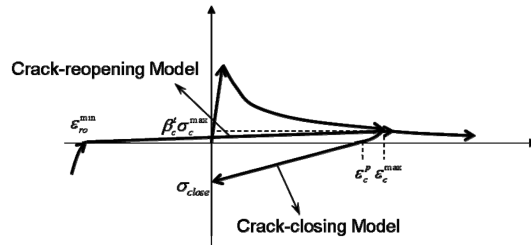


Fig. 7 Crack-closing and crack-reopening model for concrete

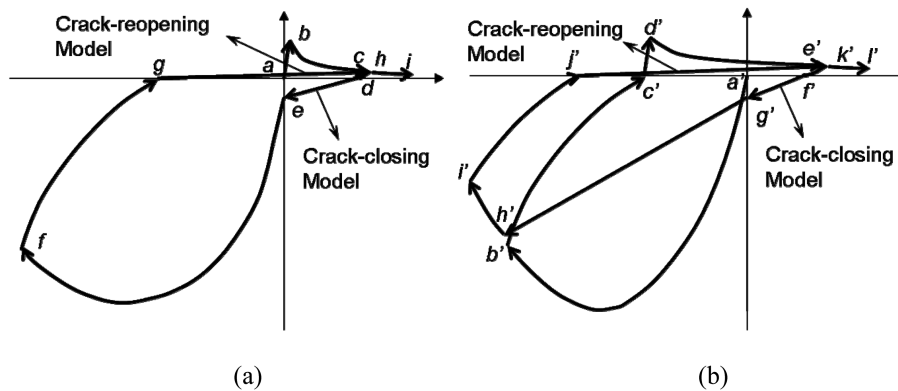


Fig. 8 Hysteretic model for reinforced concrete and its transition model: (a) Hysteretic curve starting with loading in tension (b) Hysteretic curve starting with loading in compression

is exceeded, the tension stiffening curve given by Eq. (2) governs the behavior followed from point b to c . When the loading is reversed at point c , the response follows the unloading curves given by Eq. (15) or (16), depending on the strain criteria given in Eq. (18). When the concrete stress is compressive at point d , the crack-closing model given by Eq. (19) is applied to reproduce the pinched behavior until compressive strain develops. Once it is under compressive strain, it follows the compressive curve from point e to f given by Eq. (6) or (10) depending on the stress state. When the loading is reversed at point f , it follows the non-linear unloading curve given by Eq. (12) to point g . Once it is back to tensile regime again from point g to h , the response follows the crack-reopening model given by Eq. (20). From point h , the tension stiffening model is used again.

However, under general loading conditions, loading might start with significant compressive loading up to crushing of the concrete and then reverse to the tensile regime. For this case, the hysteresis model is described in Fig. 8(b). Because there is limited experimental data to formulate the response in this extreme case, the tensile envelope curve is assumed to be shifted to the compressive plastic offset strain without degradation. First, it follows compressive behavior from point a' to b' . Once loading is reversed at point b' , the concrete response follows the non-linear unloading curve from point b' to point c' and then the concrete is subjected to tensile stress. From point c' to d' , linear elastic behavior governs the response till the cracking stress is reached at point d' . Beyond the cracking stress, tension stiffening behavior occurs until point e' and then if the loading is reversed at point e' , it follows the unloading response curves to point f' depending on the strain criteria as mentioned in Fig. 8(a). The crack-closing process starts when the stress becomes compressive. Therefore, from point f' to point g' , it follows the crack-closing model. Once negative

strain develops, a linear elastic reloading model with stiffness degradation is applied from point g' to h' until the strain reaches the current minimum unloading strain. Beyond the minimum unloading strain point h' , softening behavior occurs until point i' . If the loading is reversed at point i' , it follows the non-linear unloading curve again from point i' to j' . If tensile stress develops beyond point j' , the crack-reopening model is used up to the maximum unloading strain, point k' . With further tensile loading, the tension stiffening curve follows from point k' through point l' .

4. Material model for steel reinforcement

For modeling cyclic behavior of the embedded reinforcement, the Monti-Nuti (1992) plasticity model is used in this study. Although its advantage is that it can consider inelastic buckling of the reinforcement, inelastic buckling is not considered here because the crack width is unknown in the proposed model. In this model, every material parameter is updated after each load reversal. Therefore, the half-cycle loading or unloading branch is described as an analytical expression in terms of the dimensionless stress and strain as (Menegotto and Pinto 1973)

$$\sigma^* = b\varepsilon^* + \frac{(1-b)\varepsilon^*}{[(1+\varepsilon^{*R})^{1/R}]} \quad (22)$$

where

$$\varepsilon^* = \frac{\varepsilon - \varepsilon_r^n}{\varepsilon_y^{n+1} - \varepsilon_r^n} \quad \text{and} \quad \sigma^* = \frac{\sigma - \sigma_r^n}{\sigma_y^{n+1} - \sigma_r^n} \quad (23)$$

and

$$R = R_0 - \frac{A_1 \xi_{\max}}{A_2 + \xi_{\max}} \quad (24)$$

and b indicates the hardening slope for the hardening branch, R is the curvature parameter, A_1 and A_2 are the material parameters and ξ_{\max} is the maximum plastic excursion developed on the half-cycle unloading or loading branch. As initial parameters for R and b , $R_0=20.0$ and $b_0=0.04$ are assumed and $A_1=16.5$ and $A_2=1.0 \times 10^{-4}$ are assumed. For the 1st cycle, stresses and strains at the reversal points and the yield stresses are illustrated in Fig. 9.

For the Bauschinger effect, only linear kinematic hardening is considered in this study. The evolutionary equation of the yield stress is described as

$$\sigma_y^{n+1} = \sigma_y^0 \text{sign}(-\xi_p^n) + \Delta\sigma_K^n \quad (25)$$

where σ_y^0 is the initial yield stress and n indicates the n th reversal. The second term on the right-hand side can be obtained from a yield function $F[\sigma_{ij}, \kappa(\varepsilon_{ij}^p)]$ with conditions $\partial F/\partial \sigma = 1$ and $\partial F/\partial \kappa = 1$ (Monti and Nuti 1992). The yield stress in Eq. (25) is linearly related to the plastic excursion, ξ_p^i

$$\Delta\sigma_K^n = \sum_{i=1}^n bE\xi_p^i \quad (26)$$

where ξ_p^i is the plastic excursion in i th half-cycle, E is the elastic modulus and b is the hardening

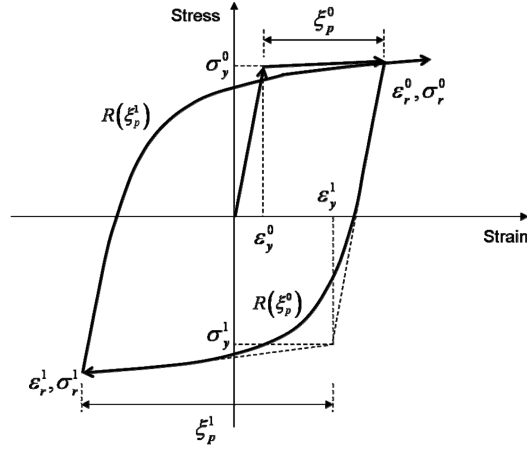


Fig. 9 Cyclic model for embedded steel reinforcement

slope.

5. Formulation of constitutive model for non-linear finite element analysis

For finite element analysis, the proposed material model is implemented into a 2D plane stress finite element. The reinforced concrete is assumed to be an orthotropic material in which the constitutive model is defined separately in two principal strain directions. In this study, regular Newton-Raphson iteration method is applied for solving the nonlinear equilibrium equation. The tangent stiffness formulation is adopted since it is more effective than the secant stiffness formulation for general loading conditions. In the global Newton-Raphson iterative process, the calculation of internal resisting forces in element level is the primary source of non-linearities because the internal resisting forces are mostly dictated by the material constitutive law. Therefore, the unbalanced force comes from the difference between external loads and internal resisting forces as in the following equation

$$\mathbf{K}_t \Delta \mathbf{U}_{n+1} = \mathbf{P}_{n+1} - \mathbf{I}_{n+1}^{(k-1)} = \mathbf{P}_{n+1} - \sum \int \mathbf{B}^T \boldsymbol{\sigma} dv \quad (27)$$

where \mathbf{K}_t is the global tangent stiffness matrix, \mathbf{P}_{n+1} is the total external loading vector at n th load step, $\mathbf{I}_{n+1}^{(k-1)}$ is the internal resisting force vector at the $(k-1)$ th iteration step in n th load step, and \mathbf{B} is the strain-displacement matrix. The global tangent stiffness is assembled from the material tangent stiffness matrices as

$$\mathbf{K}_t = \sum_{i=1}^{n \text{ elem}} \int_{v_i} \mathbf{B}^T \mathbf{D}_{n+1}^{(k)} \mathbf{B} dv \quad (28)$$

where 'n elem' indicates the total number of elements and \mathbf{B} is the strain-displacement matrix. Material constitutive model in terms of incremental stress and strain can be expressed as

$$\begin{Bmatrix} \Delta\sigma_{c1} \\ \Delta\sigma_{c2} \\ \Delta\sigma_{c12} \end{Bmatrix} = \mathbf{D}_{n+1}^{(k)} \begin{Bmatrix} \Delta\varepsilon_{c1} \\ \Delta\varepsilon_{c2} \\ \Delta\varepsilon_{c12} \end{Bmatrix} \quad (29)$$

where $\mathbf{D}_{n+1}^{(k)}$ is the algorithmic material tangent stiffness matrix at the $(n+1)$ th load step and (k) th iterative step in the principal direction and $\Delta\sigma_{ci}$ and $\Delta\varepsilon_{ci}$ are the increments of the principal stress and strain. The material tangent stiffness is calculated based on the current stress state. For example, under biaxial compression (in 1-direction) and tension (2-direction) state, the algorithmic material stiffness matrix is not symmetric as in the following equation

$$\mathbf{D}_{n+1}^{(k)} = \frac{\partial(\boldsymbol{\sigma}_{n+1}^{(k)} - \boldsymbol{\sigma}_n)}{\partial(\boldsymbol{\varepsilon}_{n+1}^{(k)} - \boldsymbol{\varepsilon}_n)} = \begin{bmatrix} \frac{\partial\Delta\sigma_{c1}}{\partial\Delta\varepsilon_{c1}} & \frac{\partial\Delta\sigma_{c1}}{\partial\Delta\varepsilon_{c2}} & 0 \\ \frac{\partial\Delta\sigma_{c2}}{\partial\Delta\varepsilon_{c1}} & \frac{\partial\Delta\sigma_{c2}}{\partial\Delta\varepsilon_{c2}} & 0 \\ 0 & 0 & \frac{1}{2} \frac{\partial(\sigma_{c1} - \sigma_{c2})}{\partial(\varepsilon_{c1} - \varepsilon_{c2})} \end{bmatrix} \quad (30)$$

where $\mathbf{D}_{n+1}^{(k)}$ is the algorithmic material tangent stiffness matrix at $(n+1)$ th load step and (k) th iterative step in the principal direction; $\Delta\sigma_{ci}(= \sigma_{n+1,ci}^{(k)} - \sigma_{n,ci})$ and $\Delta\varepsilon_{ci}(= \varepsilon_{n+1,ci}^{(k)} - \varepsilon_{n,ci})$ are the increments of the principal stress and strain. The off-diagonal term is attributed to softening or confining effect of the concrete under biaxial stress states. When stress is under compression in the 2-direction, $\mathbf{D}_{n+1}^{(k)}(1,2) = 0$ and $\mathbf{D}_{n+1}^{(k)}(1,2) = \partial\Delta\sigma_{c2}/\partial\Delta\varepsilon_{c1}$. However, in the case of biaxial tension or compression stress states, the material tangent stiffness matrix becomes a diagonal matrix. Although there is no shear stiffness in the case of this rotating crack model, the shear stiffness is necessary for the computation of the element stiffness. Thus, following the previous studies (Crisfield and Wills 1989, Stevens, *et al.* 1991b, Willam, *et al.* 1987), the shear stiffness is calculated in Eq. (30). After updating the material stiffness matrix at each iterative step, it is rotated as follows

$$\bar{\mathbf{D}}_{n+1}^{(k)} = \mathbf{R}^T \mathbf{D}_{n+1}^{(k)} \mathbf{R} \quad (31)$$

where $\bar{\mathbf{D}}_{n+1}^{(k)}$ is the material stiffness matrix in the elemental local coordinate system and \mathbf{R} is the transformation matrix from principal direction to elemental coordinate system given by

$$\mathbf{R} = \begin{bmatrix} CC & SS & CS \\ SS & CC & -CS \\ -2CS & 2CS & CC-SS \end{bmatrix} \quad (32)$$

where $C=\cos(\theta_p)$ and $S=\sin(\theta_p)$ and θ_p is the angle between the principal direction and elemental local coordinate system as shown in Fig. 10.

Steel reinforcement is modeled by smeared layers. The tangent material stiffness matrix must also be rotated to the elemental coordinate system before elemental stiffness matrices are numerically integrated

$$\mathbf{D}_{steel,i} = \begin{bmatrix} \rho_i E_i & 0 & 0 \\ 0 & 0 & 0 \\ 0 & 0 & 0 \end{bmatrix}; \mathbf{D}_{steel} = \sum_{i=1}^{n \text{ rebar}} \mathbf{R}^T \mathbf{D}_{steel,i} \mathbf{R} \quad (33)$$

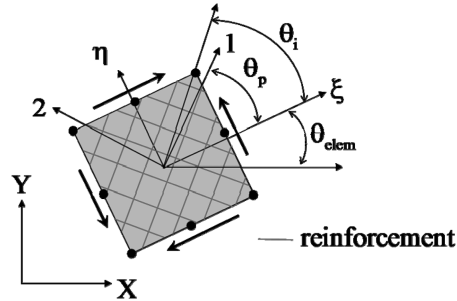


Fig. 10 Coordinate systems for 8-Node 2D planar reinforced concrete finite element

where ρ_i is the steel ratio; E_t is the tangential modulus of the reinforcement and ‘ n rebar’ is the total number of reinforcement groups. \mathbf{R} is given in Eq. (32) but the angle θ_p is replaced by θ_i shown in Fig. 10. Then the total material stiffness matrix for reinforced concrete is calculated as the sum of reinforcement and concrete stiffness.

The solution strategy for non-linear finite element analysis with the proposed model is illustrated in Fig. 11. At the material level, the total strain increments at the current load step are given to a material package. Based on the total strains, the principal strains and their directions are calculated. The concrete stress-strain constitutive relationship is determined for updating the current stress by

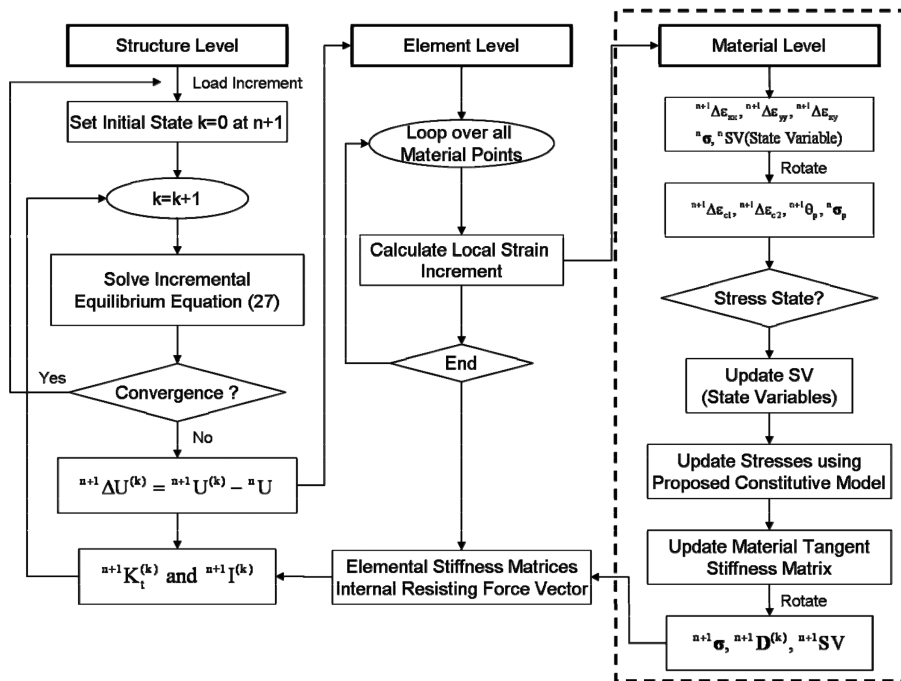


Fig. 11 Solution strategy for non-linear finite element analysis with proposed total strain-based material constitutive model for reinforced concrete

considering the current state variables and stress states at the last convergence point. The state variables are defined as variables used to keep track of hysteretic behavior. They include maximum and minimum stress and strain at load reversal points along the stress-strain curves, damage indicators and strain offset for the tensile backbone curve, etc. Following the proposed model, principal stress components are calculated. Based on the stress increments in the principal direction, the tangent material stiffness matrix is calculated as in Eq. (30). Before assembling the elemental stiffness matrices, the material stiffness matrices are rotated back to each elemental coordinate system.

6. Verification of the proposed model

The proposed model is verified by comparing its predictions with existing experimental data. The primary objectives in this experimental verification are: 1) to verify the predictive capabilities of the proposed model with respect to the behavior of the reinforced panels tested under in-plane cyclic loading; 2) to perform a parametric study to investigate the effects of the crack-closing model on the prediction of strength and pinched behavior; and, 3) to perform a study to compare the proposed model and a existing hysteretic model which uses a secant stiffness-based unloading and reloading scheme. Recently, it was reported that orientation of the reinforcement in an RC shear panel has a significant effect on the level of pinching in post-yielding responses (Mansour and Hsu 2005a). To investigate the performance of the proposed model, two RC shear panels tested by Hsu, *et al.* (2005a) have been chosen and their experimental results are compared with the results generated by non-linear finite element analysis using the proposed model. Primary variables for the three RC

Table 1 Physical properties of tested RC shear panels

Panel	Concrete		Steel in longitudinal direction			Steel in transverse direction			α (degree)
	f'_c (MPa)	ϵ_0	Rebars	ρ_t	f_{yt} (MPa)	Rebars	ρ_t	f_{yt} (MPa)	
CE3	50	0.0024	# 6 at 267 mm	0.012	425.4	# 6 at 267 mm	0.012	425.4	90
CA3	44.5	0.0024	# 6 at 188 mm	0.017	425.4	# 6 at 188 mm	0.017	425.4	45

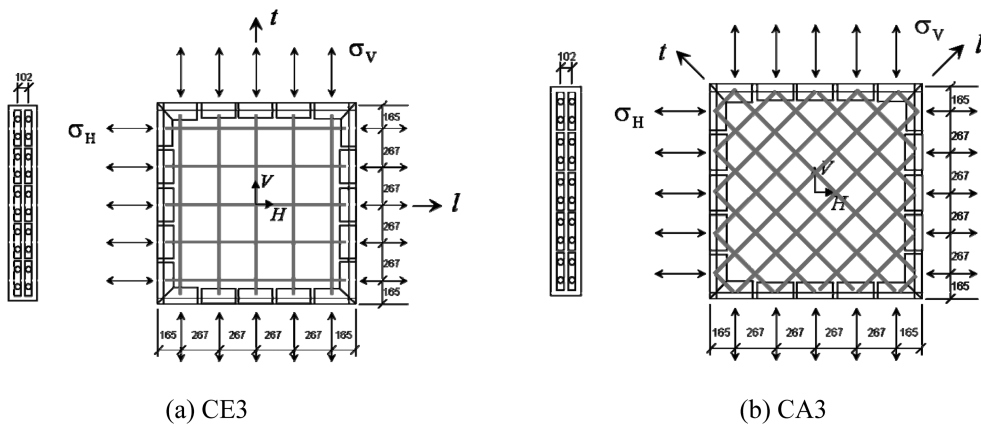


Fig. 12 Steel arrangement of RC shear panel CE3 (90 degree) and CA3 (45 degree)

shear panels are summarized in Table 1. Embedded reinforcements and geometric dimensions are illustrated in Fig. 12. The RC panels are tested under mixed loading control scheme in which loading is applied in stress-control mode and then with strain-control mode after yielding occurred. However, strain histories re-sampled from the experimental data are applied for stable non-linear finite element simulation throughout the entire loading history.

6.1. Analysis results and discussion - panel CE3

Panel CE3 experiences extremely large tensile strains in principal strain directions as shown in Fig. 13. Since the orientations of the reinforcements are in the principal strain directions, the total stress-strain behavior is mostly governed by reinforcement behavior in this RC panel. Two parameters related to the crack-closing model are studied in the three cases summarized in Table 2. As shown in Eq. (19), α and γ change the crack-closing stiffness. This is obviously manifested in the predicted cyclic behaviors of the concrete as shown in Fig. 14. Case III shows the least stiffness under crack-closing mechanisms while Case I shows the largest crack-closing stiffness. Fig. 15 shows comparisons of the cyclic total stress-strain behaviors for simulations and experiments. Responses in the tensile stress regime are predicted accurately for the three cases in both strength and stress-strain path. However, significant discrepancies are observed in the compressive stress regime. One of the observations from the comparison is that predicted compressive strength is proportional to the crack-closing stiffness. Case II shows the best prediction of the compressive strength. The discrepancy in the compressive stresses may be attributed to various factors such as concrete crushing and bond-slip between concrete, and reinforcement. This shows the importance of the crack-closing model in predicting behaviors of RC panels under cyclic loading. It is concluded that further study in the crack closing model is required to improve the prediction of the cyclic

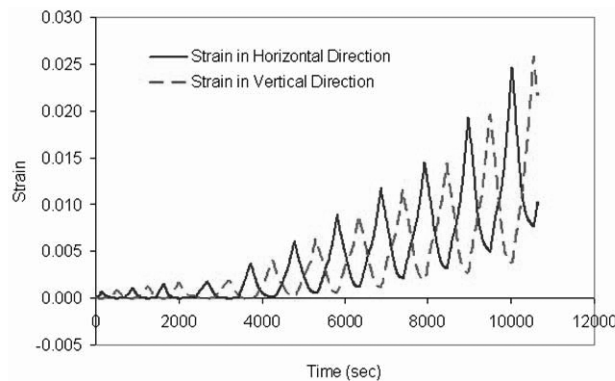


Fig. 13 Strain histories in horizontal and vertical direction for CE3 RC Panel

Table 2 Parameters for crack-closing model in Eq. (19)

	α	γ
Case I	0.0016	50×10^{-5}
Case II	0.00001	30×10^{-5}
Case III	0.00001	10×10^{-5}

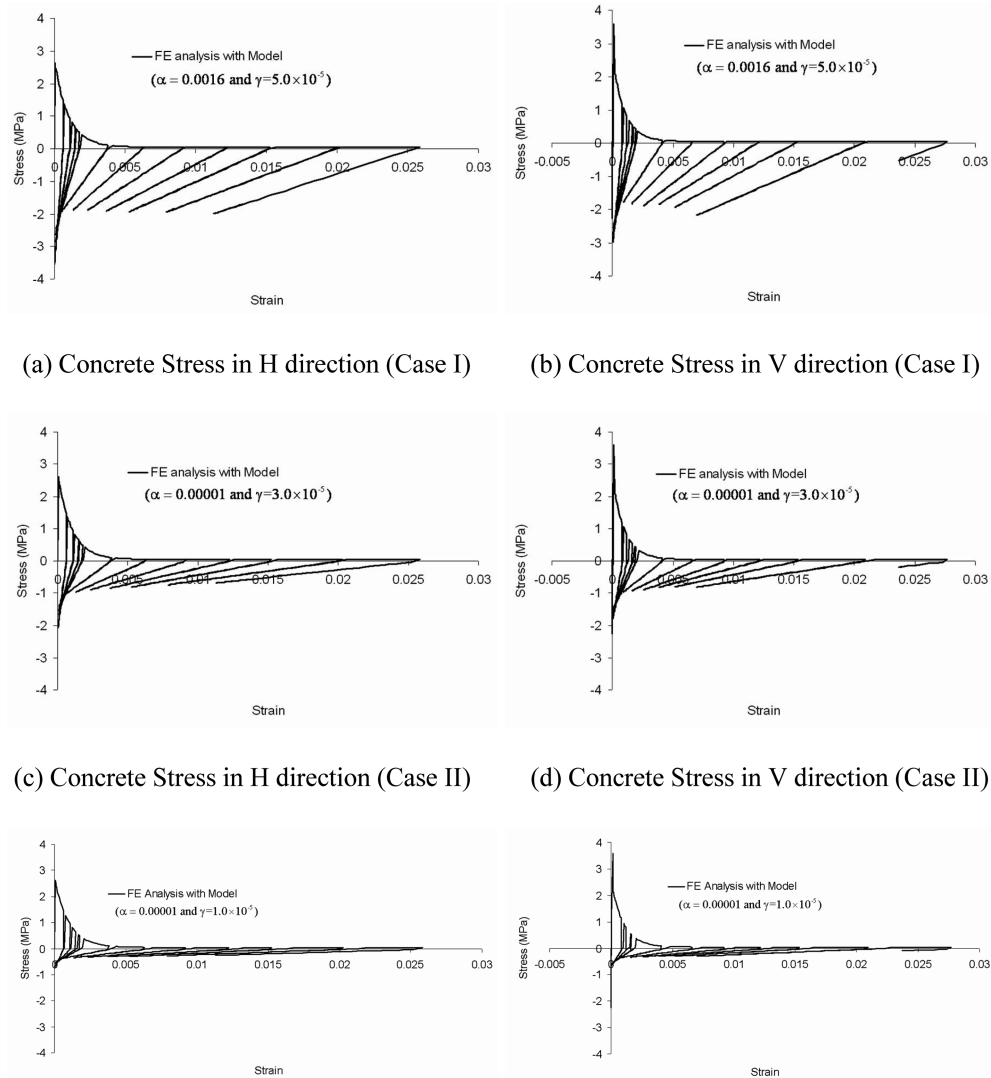


Fig. 14 Effect of α and γ on the concrete stress strain curves in longitudinal and transverse direction as predicted by the proposed constitutive model: tested panel CE3 (90 degree)

behavior.

Fig. 16 shows comparisons of the cyclic shear stress-strain behavior for the simulations and experiments. As mentioned in Mansour and Hsu (2005a), panels with 90 degree reinforcement arrangements show very stable cyclic behavior. Finite element analysis results agree with the experimental results of the panel with 90 degree reinforcements, showing very stable cyclic behavior. Comparing Case I and Case II, Case II gives better prediction of shear strength than Case I.

6.2. Analysis results and discussion - panel CA3

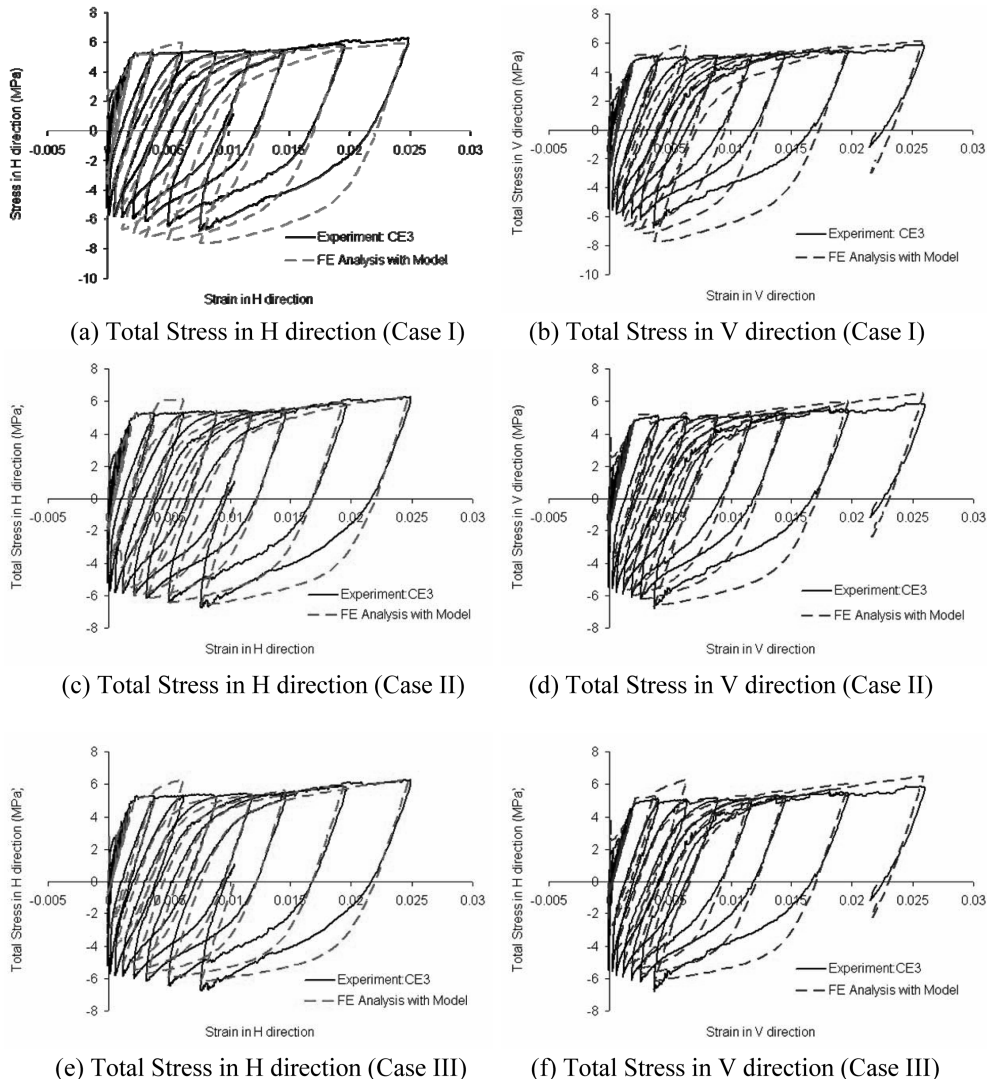


Fig. 15 Comparison of predicted total stress-strain with experiment CE3 Case I: $\alpha=0.0016$ and $\gamma=50 \times 10^{-5}$, Case II: $\alpha=0.00001$ and $\gamma=30 \times 10^{-5}$, Case III: $\alpha=0.00001$ and $\gamma=10 \times 10^{-5}$

The reinforcements for panel CA3 is oriented 45 degrees from horizontal directions as shown in Fig. 12 (b). The first part of the strain history data was truncated to remove noise in the data as shown in Fig. 17. Hsu, *et al.* observed severe pinching in cyclic shear stress-strain responses for panels reinforced with 45 degree reinforcements. In this verification, the two cases, Case I and II, developed for panel CE4 was used to investigate the effect of the crack-closing stiffness on the predicted responses. Fig. 18 shows the cyclic stress-strain response of the concrete. Compressive stresses in Case II after cracks are completely closed are lower than those in Case I. It is notable that compressive strength under large tensile strains in the direction orthogonal to compressive direction is reduced based on the modified compression field theory described in Section 3.2.1.

Fig. 19 compares the total stress-strain behavior for FE analysis with experimental data. The

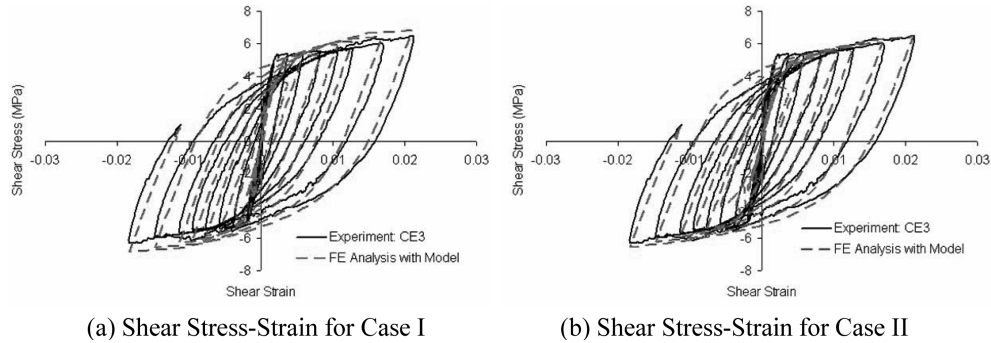


Fig. 16 Comparison of cyclic shear stress-strain curves with experimental data CE3

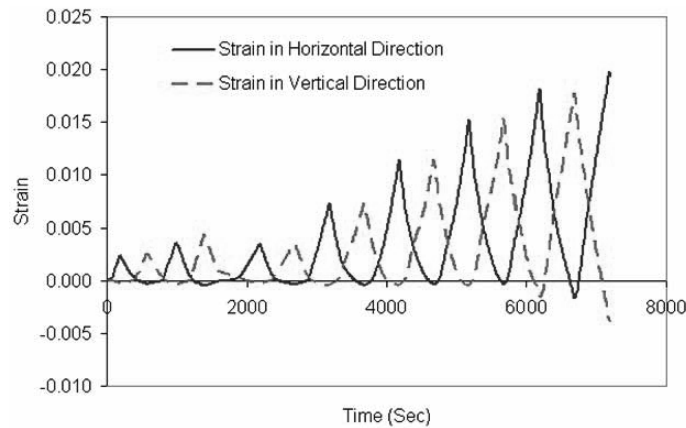


Fig. 17 Strain histories in horizontal and vertical direction for CA3 RC Panel

proposed model gives rational predictions of the tensile strength in the last five cycles both in horizontal and vertical directions. However, discrepancies are clear in the prediction of compressive stresses. The primary reason for the discrepancy is the simplified crack-closing model using linear elastic stiffness. Case II gives less compressive stresses during cracking-closing process than case I. Furthermore, the non-smooth transition from tensile strains to compressive strains of the proposed model also renders obvious discrepancies with the experimental data.

Fig. 20 compares the simulated cyclic shear stress-strain relationship to the experimental results. The proposed model reasonably predicts the shear strength in the last four cycles. A comparison between Cases I and II in Fig. 20 demonstrates the importance of the crack-closing model in reproducing the pinched shear stress-strain relationship, that is, Case I with a larger crack-closing stiffness results in more energy dissipation in cyclic shear stress-strain curves than Case II. One of the observations from Fig. 20 is that the proposed model could not predict the first yielding points in both loading directions. It is due to the fact that the average stress of embedded steel bars is quite different from the stress in the bare steel (Belarbi and Hsu 1994, Mansour, *et al.* 2001). The steel model used in this paper does not consider the effect of embedment of steel bars. Thus, the prediction of the first yielding points can be improved.

The proposed hysteretic model for RC structures is compared with the secant unloading stiffness-based hysteretic model in Fig. 21 and Fig. 22. For the secant unloading stiffness-based hysteretic

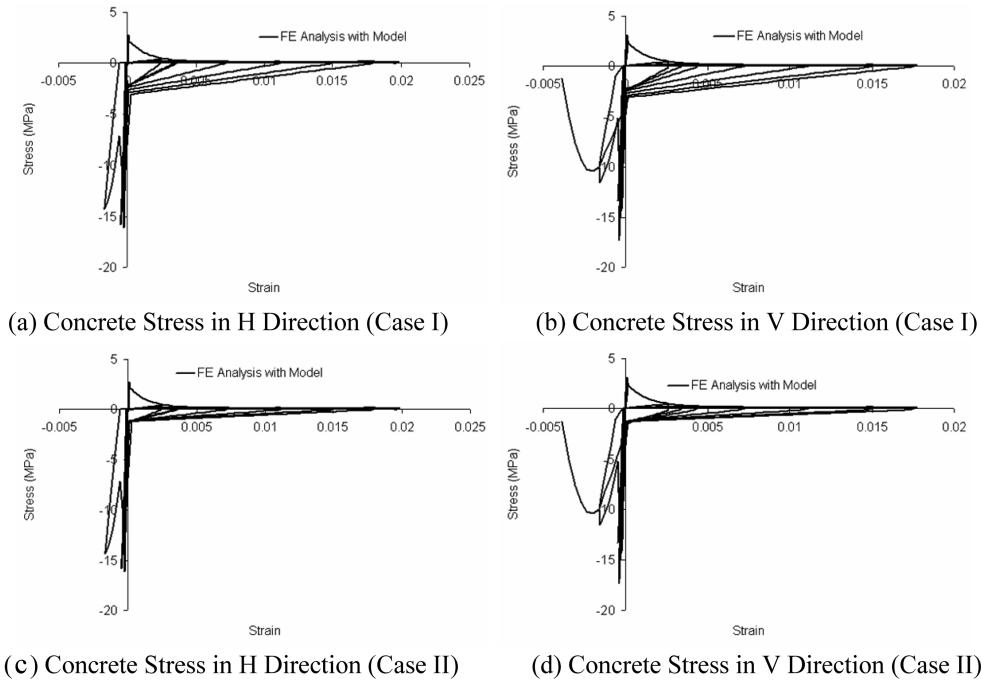


Fig. 18 Effect of α and γ on the concrete stress strain curves in longitudinal and transverse direction as predicted by the proposed constitutive model: Tested Panel CA3 (45 degree)

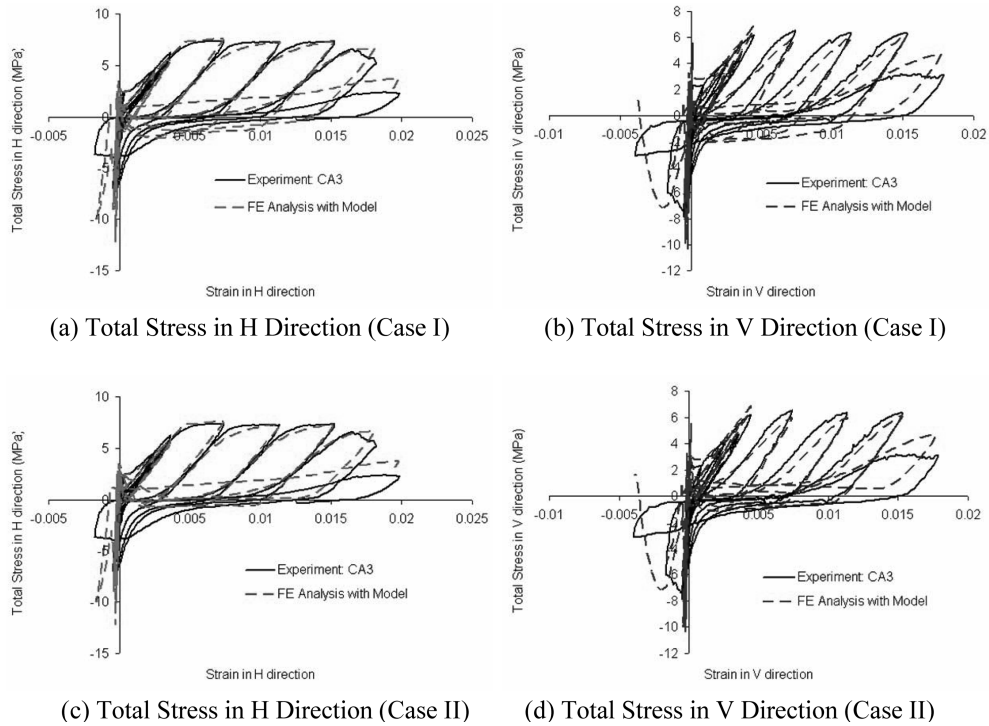


Fig. 19 Comparisons of predicted total stress with experiment CA3

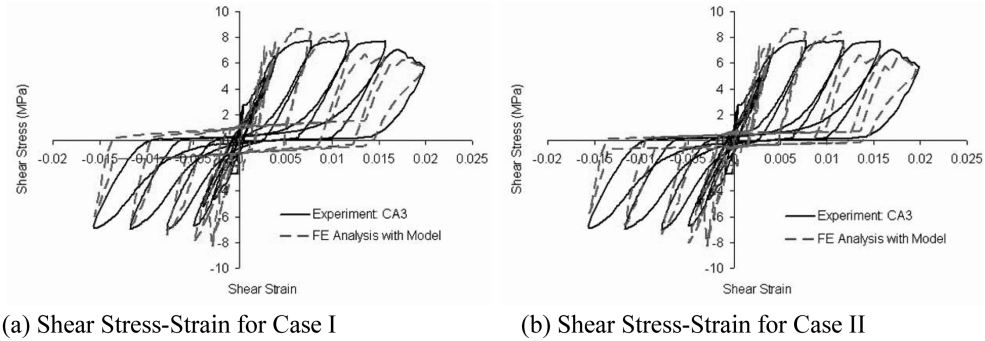


Fig. 20 Comparison of cyclic shear stress-strain curves with experimental data CA3

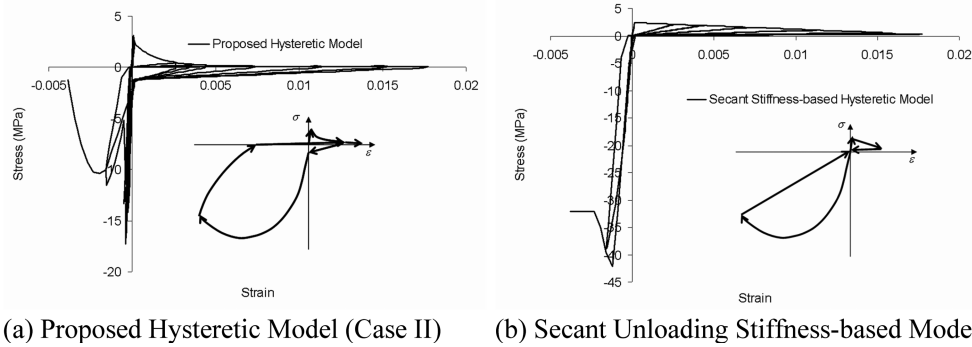


Fig. 21 Comparisons of concrete stress-strain relationship for the proposed hysteretic model and secant unloading stiffness-based model

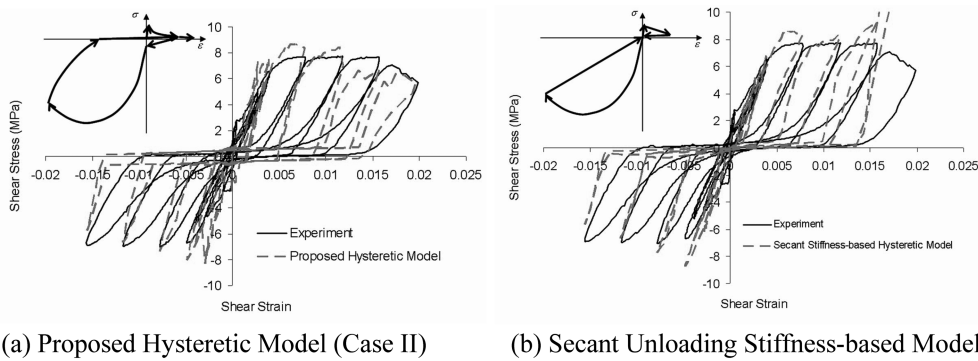


Fig. 22 Comparison of cyclic shear stress-strain curves for the proposed hysteretic model and secant unloading stiffness-based model

model, compressive behavior of the concrete is modeled by a plasticity model based on the Drucker-Prager model with a non-associate flow rule. Tensile behavior after cracking is modeled by a linear curve. However, the material stiffness is formulated based on tangent stiffness scheme not considering any plastic offset as illustrated in Fig. 21(b) and Fig. 22(b). Because the plasticity-based concrete model cannot account for continuous strength degradation under tension-compression

biaxial stress state, compressive strength is much higher for the secant unloading stiffness-based hysteretic model than for the proposed model. Fig. 22 compares cyclic shear stress-strain behavior for the two hysteretic models. Two distinct advantages of the proposed hysteretic model are: 1) more realistic energy dissipation through repeated cyclic loading, and 2) better correlation with experimental data in terms of predictions and degradation of the strength than the secant unloading stiffness-based hysteretic model.

As evidenced in the series of comparative and parametric studies, rational modeling of various damage mechanisms of reinforced concrete structures under cyclic loading conditions and their hysteretic rules for general loading conditions is important for accurate prediction of various responses.

7. Conclusion and further research

In this paper, a total strain-based hysteretic model for reinforced concrete structures has been proposed based on the smeared rotating crack modeling concept. For embedded reinforcements, stiffness contributions from reinforcement are accounted for by a smeared modeling concept and the Monti-Nuti plasticity model is employed for the reinforcement. The proposed model is an extension of Palermo's cyclic model for reinforced concrete structures. Additionally, an efficient tension stiffening model is implemented for practical finite element analysis and a fully generalized hysteresis rule has been suggested for reproducing various damage mechanisms such as crack-reopening, crack-closing behavior and unloading/reloading behavior under repeated cyclic loading conditions. Moreover, the proposed model uses tangent stiffness formulation in the non-linear finite element analysis instead of the secant stiffness formulation.

The main features of the proposed model are: 1) a rational tension stiffening model which can take into account the effect of reinforcement orientation and ratio on post-cracking behavior; 2) a linear or non-linear unloading curve as a function of inelastic residual strain depending on the strain level along the curve; 3) full and partial reloading curves considering strength degradation; 4) a simplified crack-closing and crack-reopening models; and, 5) a tangent stiffness formulation. The accuracy of the proposed model has been verified using available panel test results. A series of parametric studies have provided insights regarding the effect of damage model parameters and hysteresis rules on behavior. According to the parametric studies, values of two parameters in Case II ($\alpha=0.00001$ and $\gamma=30\times 10^5$) related to the crack-closing model are shown to give better correlation with experimental observations than other cases. Along with the suggested parameters, the pinching degree of cyclic shear stress and strain curves was observed to be influenced by the cracking closing and reopening model.

However, it is noteworthy that further research and understanding of various damage mechanisms under cyclic loading conditions are required to improve performance of hysteretic models for reinforced concrete structures. In particular, the impact of cyclic loading, bond slip, and shear slip along crack surfaces as well as crushing of crack surfaces need to be understood and included in material models.

Acknowledgement

This paper is based on the work supported in part by the National Science Foundation under Research Grant No. CMMI-0625640. Any opinions, findings, conclusions, or recommendations stated in this paper are those provided by the authors and do not necessarily reflect the views of the National Science and Foundation.

References

- Bahn, B. Y. and Hsu, C. T. T. (1998), "Stress-strain behaviour of concrete under cyclic loading", *ACI Mater. J.*, **95**(2), 178-193.
- Belarbi, A. and Hsu, T. T. C. (1991) *Constitutive Laws of Reinforced Concrete in Biaxial Tension Compression*, University of Houston: Houston.
- Belarbi, A. and Hsu, T. T. C. (1994), "Constitutive laws of concrete in tension and reinforcing bars stiffened by concrete", *ACI Struct. J.*, **91**(4), 465-474.
- Belarbi, A. and Hsu, T. T. C. (1995), "Constitutive laws of softened concrete in biaxial tension-compression", *ACI Struct. J.*, **92**(5), 562-573.
- Buyukozturk, O. and Tseng, T. M. (1984), "Concrete in biaxial cyclic compression", *J. Struct. Eng. ASCE*, **110**(3), 461-476.
- Chen, W. F. (1988), "Evaluation of plasticity-based constitutive models for concrete materials", *Solid Mech. Archives*, **13**(1), 1-63.
- Cotsovos, D. M. and Pavlovic, M. N. (2005), "Numerical investigation of RC structural walls subjected to cyclic loading", *Comput. Concrete*, **2**(3), 215-238.
- Crisfield, M. A. and Wills, J. (1989), "Analysis of R/C panels using different concrete models", *J. Eng. Mechanics-ASCE*, **115**(3), 578-597.
- De Borst, R. and Feenstra, P. H. (1995), "A plasticity model and algorithm for mode-I cracking in concrete", *Inter. J. Numer. Methods Eng.*, **38**, 2509-2529.
- Elmorsi, M., Kianoush, M. R., and Tso, W. K. (1998), "Nonlinear analysis of cyclically loaded reinforced concrete structures", *ACI Struct. J.*, **95**(6), 725-739.
- He, W., Wu, Y. F., Liew, K. M., and Wu, Z. S. (2006), "A 2D total strain based constitutive model for predicting the behaviors of concrete structures", *Int. J. Eng. Sci.*, **44**(18-19), 1280-1303.
- Hsu, T. T. C., Mansour, M. Y., Mo, Y. L., and Zhong, J. (2006), "Cyclic softened membrane model for nonlinear finite element analysis of concrete structures", *SP-237 ACI Finite Element Analysis of Reinforced Concrete Structures*: 71-98.
- Hsu, T. T. C. and Zhang, L. X. (1997), "Nonlinear analysis of membrane elements by fixed-angle softened-truss model", *ACI Struct. J.*, **94**(5), 483-492.
- Hsu, T. T. C. and Zhu, R. R. H. (2002), "Softened membrane model for reinforced concrete elements in shear", *ACI Struct. J.*, **99**(4), 460-469.
- Karsan, I. D. and Jirsa, J. O. (1969), "Behavior of concrete under compressive loading", *J. Struct. Div., ASCE*, **95**, 2543-2563.
- Kent, D. C. and Park, R. (1971), "Flexural members with confined concrete", *J. Struct. Div., ASCE*, **97**, 1969-1990.
- Kim, T. H., Lee, K. M., and Shin, H. M. (2002), "Nonlinear analysis of reinforced concrete shells using layered elements with drilling degree of freedom", *ACI Struct. J.*, **99**(4), 418-426.
- Kratzig, W. B. and Polling, R. (2004), "An elasto-plastic damage model for reinforced concrete with minimum number of material parameters", *Comput. Struct.*, **82**(15-16), 1201-1215.
- Kupfer, H., Hilsdorf, H. K., and Rusch, H. (1969), "Behavior of concrete under biaxial stress", *J. American Concrete Inst.*, **66**(8), 656-666.
- Kwak, H. G. and Kim, D. Y. (2004), "Material nonlinear analysis of RC shear walls subject to cyclic loadings", *Eng. Struct.*, **26**(10), 1423-1436.
- Mansour, M. and Hsu, T. T. C. (2005a), "Behavior of reinforced concrete elements under cyclic shear. I: Experiments", *J. Struct. Eng.-ASCE*, **131**(1), 44-53.
- Mansour, M. and Hsu, T. T. C. (2005b), "Behavior of reinforced concrete elements under cyclic shear. II:

- Theoretical model”, *J. Struct. Eng.-ASCE*, **131**(1), 54-65.
- Mansour, M., Lee, J. Y., and Hsu, T. T. C. (2001), “Cyclic stress-strain curves of concrete and steel bars in membrane elements”, *J. Struct. Eng.-ASCE*, **127**(12), 1402-1411.
- Menegotto, M. and Pinto, P. (1973), “Method of analysis for cyclically-loaded R/C plane frames including changes in geometry and non-elastic behavior of elements under combined normal force and bending”, in *IABSE Symposium on Resistance and Ultimate Deformability of Structures Acted on by Well-Defined Repeated Loads*. Lisbon.
- Mikame, A., Uchida, K., and Noguchi, H. (1991), “A study of compressive deterioration of cracked concrete”, in *Proceedings, International Workshop on Finite Element Analysis of Reinforced Concrete*. Columbia University, New York.
- Monti, G. and Nuti, C. (1992), “Nonlinear cyclic behavior of reinforcing bars including buckling”, *J. Struct. Eng. ASCE*, **118**(12), 3268-3284.
- Noh, H. C. and Choi, C. K. (2006), “Ultimate behavior of reinforced concrete cooling tower: Evaluation and comparison of design guidelines”, *Struct. Eng. Mech.*, **22**(2), 223-240.
- Palermo, D. and Vecchio, F. J. (2003), “Compression field modeling of reinforced concrete subjected to reversed loading: formulation”, *ACI Struct. J.*, **100**, 616-625.
- Palermo, D. and Vecchio, F. J. (2004), “Compression field modeling of reinforced concrete subjected to reversed loading: Verification”, *ACI Struct. J.*, **101**(2), 155-164.
- Palermo, D. and Vecchio, F. J. (2007), “Simulation of cyclically loaded concrete structures based on the finite-element method”, *J. Struct. Eng.-ASCE*, **133**(5), 728-738.
- Pang, X. B. D. and Hsu, T. T. C. (1996), “Fixed angle softened truss model for reinforced concrete”, *ACI Struct. J.*, **93**(2), 197-207.
- Park, H. and Kim, J. Y. (2005), “Hybrid plasticity model for reinforced concrete in cyclic shear”, *Eng. Struct.*, **27**(1), 35-48.
- Scott, B. S., Park, R., and Priestley, M. J. N. (1982), “Stress strain behavior of concrete confined by overlapping hoops at low and high strain rates”, *ACI Struct. J.*, **79**(1), 13-27.
- Stevens, N. J., Uzumeri, S. M., and Collins, M. P., *Analytical Modeling of Reinforced Concrete Subjected to Monotonic and Reversed Loadings*. 1987, Department of Civil Engineering, University of Toronto: Toronto. p. 201.
- Stevens, N. J., Uzumeri, S. M., and Collins, M. P. (1991a), “Reinforced-concrete subjected to reversed cyclic shear - experiments and constitutive model”, *ACI Struct. J.*, **88**(2), 135-146.
- Stevens, N. J., Uzumeri, S. M., Collins, M. P., and Will, G. T. (1991b), “Constitutive model for reinforced-concrete finite-element analysis”, *ACI Struct. J.*, **88**(1), 49-59.
- Vecchio, F. J. (1992), “Finite-element modeling of concrete expansion and confinement”, *J. Struct. Eng.-ASCE*, **118**(9), 2390-2406.
- Vecchio, F. J. (1999), “Towards cyclic load modeling of reinforced concrete”, *ACI Struct. J.*, **96**(2), 193-202.
- Vecchio, F. J. and Collins, M. P. (1986), “The modified compression field theory for reinforced concrete elements subjected to shear”, *ACI Struct. J.*, **83**(2), 219-231.
- Wang, T. J. and Hsu, T. T. C. (2001), “Nonlinear finite element analysis of concrete structures using new constitutive models”, *Comput. Struct.*, **79**(32), 2781-2791.
- Willam, K., Pramono, E., and Sture, S. (1987), “Fundamental issues of smeared crack models”, *Proceedings of the SEM-RILEM International Conference on Fracture of Concrete and Rocks*. Houston, Texas.
- Yankelevsky, D. Z. and Reinhardt, H. W. (1989), “Uniaxial behavior of concrete in cyclic tension”, *J. Struct. Eng. ASCE*, **115**(1), 166-182.
- Zhang, L. X. B. and Hsu, T. T. C. (1998), “Behavior and analysis of 100 MPa concrete membrane elements”, *J. Struct. Eng.-ASCE*, **124**(1), 24-34.
- Zhong, J. (2005) “*Model-Based Simulation of Reinforced Concrete Plane Stress Structures*”, in Department of Civil Engineering, University of Houston: Houston. Ph.D. thesis
- Zhu, R. R. H., Hsu, T. T. C., and Lee, J. Y. (2001), “Rational shear modulus for smeared-crack analysis of reinforced concrete”, *ACI Struct. J.*, **98**(4), 443-450.